Japanese Journal of Radiology
https://doi.org/10.1007/s11604-025-01936-w

ORIGINAL ARTICLE

Time-dependent diffusion-weighted imaging assessment of tumor grading and *isocitrate dehydrogenase* genotypes in adult-type diffuse gliomas

Kiyohisa Kamimura[1] · Tsubasa Nakano[2] · Masanori Nakajo[2] · Junki Kamizono[2] · Tomohito Hasegawa[2] · Daiki Tobo[2] · Akie Mukai[2] · Yoshiki Kamimura[2] · Fumitaka Ejima[2] · Hiroaki Nagano[2] · Koji Takumi[2] · Masatoyo Nakajo[2] · Nayuta Higa[3] · Hajime Yonezawa[3] · Ryosuke Hanaya[3] · Mari Kirishima[4] · Akihide Tanimoto[4] · Hirokazu Otsuka[5] · Daisuke Hirahara[6] · Hiroshi Imai[7] · Thorsten Feiweier[8] · Takashi Yoshiura[1]

Received: 10 September 2025 / Accepted: 7 December 2025

Abstract

Background This study aimed to investigate the usefulness of time-dependent diffusion magnetic resonance imaging (MRI) parameters compared with the conventional apparent diffusion coefficient (ADC) in distinguishing tumor grade and isocitrate dehydrogenase (IDH) genotypes of adult-type diffuse gliomas.

Methods This retrospective study included 102 patients with adult-type diffuse gliomas. ADC maps obtained using diffusion-weighted imaging at short (7.1 ms) and long (44.5 ms) diffusion times (ADC7.1ms and ADC44.5ms) and maps of ADC changes (cADC) and relative ADC changes (rcADC) between the two diffusion times were generated. The mean, 5th, and 95th percentile values of each parameter were compared between low-grade (LGGs) and high-grade gliomas (HGGs) and between IDH-mutant and IDH-wildtype gliomas. The discriminative performance was assessed using receiver operating characteristic (ROC) analysis, and correlation with Ki-67 labeling index (Ki-67LI) was assessed using Spearman's rank correlation. Multivariable logistic regression analyses were conducted to predict HGGs and IDH-wildtype gliomas.

Results In HGGs, the mean and 5th percentile values of ADC44.5ms and ADC7.1ms were significantly lower, whereas cADC and rcADC indices were significantly higher than those in LGGs. Performance of the mean rcADC (area under the ROC curve: 0.925; 95% confidence interval: 0.855–0.967) was significantly better than any index of conventional ADCs for tumor grade classification. The mean rcADC demonstrated the strongest correlation with Ki-67LI ($\rho = 0.542$, $p < 0.0001$). Moreover, the 95th percentile of rcADC was an independent predictor of IDH-wildtype gliomas after adjustment for age and sex, was useful for distinguishing IDH-wildtype from IDH-mutant gliomas

Conclusions The mean rcADC showed the strongest correlation with the Ki-67 LI and achieved better diagnostic performance than conventional PGSE-based ADC for differentiating LGGs from HGGs. In multivariable analyses, the mean and 95th percentile of rcADC were identified as independent predictors of HGGs and IDH-wildtype gliomas, respectively.

Keywords Adult-type diffuse glioma · *Isocitrate dehydrogenase* genotypes · MRI · Time-dependent diffusion · Tumor grading

Introduction

Adult-type diffuse gliomas account for a large proportion of primary brain tumors and remain challenging to diagnose and treat. Traditionally, these tumors have been classified as low-grade gliomas (LGGs) and high-grade gliomas (HGGs) according to their histological features, with LGGs generally associated with a more favorable prognosis [1]. The fifth edition of the World Health Organization (WHO) Classification of Tumors of the Central Nervous System emphasizes the importance of molecular and genetic profiles in the diagnosis of diffuse gliomas [2]. The mutation status of the

Extended author information available on the last page of the article

Published online: 05 January 2026

isocitrate dehydrogenase (IDH) gene is a crucial factor in tumor development. The *IDH*-mutant gliomas demonstrate a less aggressive biological behavior and are more responsive to chemotherapy, which is related to a more favorable prognosis [3]. Moreover, patients whose tumors have chromosome arms 1p and 19q codeletion (*1p/19q* codeletion) a feature that is frequently observed in oligodendroglioma survive longer than those with tumors that lack this deletion [4]. A small number of *IDH*-mutant gliomas are classified as HGGs, making the differentiation between LGGs and HGGs equally important [2]. The Ki-67 labeling index (LI), a marker of tumor cell proliferation, is strongly associated with tumor differentiation, invasiveness, and patient prognosis [5, 6]. A previous study has revealed the Ki-67 LI as a crucial prognostic factor in astrocytomas [7]. Biopsy and histopathological analysis are the gold standard for glioma classification and molecular feature detection [2]. However, these procedures are invasive and may lead to sampling errors due to intratumoral heterogeneity [8]. Conventional MRI is a noninvasive technique; however, it only provides limited information for an accurate diagnosis [9−13].

Diffusion-weighted imaging (DWI) and apparent diffusion coefficient (ADC) measurements provide important information about microstructural organization. ADC values exhibit an inverse correlation with tumor cellularity [9]. Studies have demonstrated significantly higher ADC values obtained from DWI for patients with LGG than those with HGG due to lower cellularity and a reduced nuclear-to-cytoplasmic ratio thereby enabling the use of DWI for glioma grading [10−13]. Moreover, the ADC values are significantly higher for *IDH*-mutant glioma than for *IDH*-wildtype glioma [14−16]. Conversely, *1p/19q* codeletion status, the ADC value remains unidentified [14−16]. Diffusion time is a fundamental parameter in DWI and represents the observation time of diffusion. Spatial barriers, such as cell membranes, restrict the movement of water molecules (restricted diffusion) in biological tissues. Under these conditions, ADC values increase as the diffusion time decreases [17–20], since a shorter diffusion time reduces the likelihood of molecular collisions with these barriers. Conventional pulsed-gradient spin-echo (PGSE) DWI sequences require a long diffusion time to attain high b-values because of the limitation in maximum gradient strength [21, 22]. Moreover, the 180° pulse lasts several milliseconds; thus, the diffusion time in PGSE has a lower limit, even if the gradient strength is unrestricted. Thus, investigating the effect of diffusion time on ADCs using a clinical MRI scanner is challenging. The oscillating-gradient spin-echo (OGSE) DWI sequence is a novel diffusion encoding technique [17] that uses rapidly oscillating gradients instead of the prolonged diffusion-sensitizing gradients utilized in the PGSE method, thereby enabling shorter diffusion times. Studies have investigated the diffusion time dependence of the ADC by combining the PGSE and OGSE methods, which is an approach known as time-dependent diffusion MRI [23–27]. Time-dependent diffusion MRI can provide additional information about restricted diffusion within the tissue microstructure.

To the best of our knowledge, no previous study has evaluated how diffusion time affects the diagnostic performance of ADC for distinguishing *IDH*-mutant from *IDH*-wildtype adult-type diffuse gliomas. Only one study has reported the differentiation of low- and high-grade intra-axial brain tumors using time-dependent diffusion MRI [24]. The present study extends the scope by investigating the correlations between time-dependent diffusion MRI parameters and a broader range of tumor characteristics, including pathology, grade, *IDH* mutation status, *1p/19q* codeletion, and Ki-67 expression. Further, this study aims to assess the potential of time-dependent diffusion MRI in distinguishing not only LGGs from HGGs but also *IDH*-mutant from *IDH*-wildtype gliomas.

Materials and methods

Patients

Our institutional review board (approval no. 220126), which waived the requirement for written informed consent due to its retrospective design, approved this study. This study included consecutive cases of pathologically confirmed adult-type diffuse gliomas that were classified according to the 2021 CNS WHO classification [2] at our institution from January 2019 to December 2024. The exclusion criteria were (a) absence of preoperative MRI, including DWI with both OGSE and PGSE sequences; (b) inadequate image quality; or (c) history of surgical resection or irradiation. The largest tumor was subject to analysis for patients with multiple lesions.

Pathological/molecular diagnosis

All *IDH*-mutant and *1p/19q*-codeleted, *IDH*-mutant, and *IDH*-wildtype adult-type diffuse gliomas were diagnosed employing an integrated approach that combined histological assessment with a glioma-tailored next-generation sequencing panel that was developed at our institution [28]. The Ki-67 LI was quantified with immunohistochemical staining and defined as the percentage of malignant cell nuclei demonstrating positive staining [7]. The glioblastomas, *IDH*-wildtype, were classified as CNS WHO grade 4; astrocytomas, *IDH*-mutant, were classified as CNS WHO

grade 2, 3, or 4; and oligodendrogliomas, *IDH*-mutant and *1p/19q*-codeleted, were classified as CNS WHO grade 2 or 3.

MRI acquisition

All patients underwent imaging using a 3T MR scanner (MAGNETOM Prisma; Siemens Healthineers AG, Forchheim, Germany) equipped with a 20-channel head-neck radiofrequency receive coil, featuring a maximum gradient amplitude of 80 mT/m and a maximum slew rate of 200 T/m/s for each gradient axis. Moreover, DWI was acquired using research sequences for OGSE DWI with b-values of 0 and 1,500 s/mm² (number of averages: 1 and 4, respectively) and three diffusion encoding directions. OGSE diffusion encoding was performed using trapezoid-sine waveforms [29]. An effective diffusion time (Δ_{eff}) of 7.1 ms (frequency = 50 Hz; diffusion gradient pulse duration [δ] = 8.5 ms) was applied. Moreover, PGSE DWI was obtained with b-values of 0 and 1,500 s/mm² (number of averages: 1 and 4, respectively) and three diffusion encoding directions. The Δ_{eff} for the PGSE encoding was 44.5 ms (with a diffusion gradient separation [Δ] of 59.8 ms and δ of 46.1 ms). Both sequences were acquired utilizing the same parameters: repetition time (TR), 4,600 ms; echo time (TE), 120 ms; field of view (FOV), 230 × 230 mm^2; matrix size, 72 × 72; and slice thickness, 5 mm. The acquisition times were 1 min 31 s for PGSE DWI and 1 min 39 s for OGSE DWI. Supplementary Fig. 1 illustrates the pulse sequence diagrams for both PGSE and OGSE.

Precontrast fluid-attenuated inversion recovery (FLAIR) images and postcontrast 2D T1-weighted spin-echo images were acquired (Supplementary Table 1). These images served as an anatomical reference for delineating regions of interest (ROIs). Our standard MRI protocol for central nervous system lesions included precontrast sequences as follows: 2D T1-weighted spin-echo imaging, 2D T2-weighted turbo spin-echo imaging, and 3D susceptibility-weighted imaging. The precontrast T1-weighted images were utilized to confirm contrast enhancement.

Creating diffusion parametric maps

ADC values were measured following the assumption of mono-exponential signal decay between lower and higher b-values.

The ADC change (cADC) and relative ADC change (rcADC) between OGSE (short diffusion time) and PGSE (long diffusion time) were assessed based on previous studies [23, 24]. The pixel-by-pixel calculations were performed to develop cADC and rcADC maps using the following formulas:

$$\mathrm{cADC} = \mathrm{ADC}_{7.1\mathrm{ms}} - \mathrm{ADC}_{44.5\mathrm{ms}}$$

$$\mathrm{rcADC} = \frac{(\mathrm{ADC}_{7.1\mathrm{ms}} - \mathrm{ADC}_{44.5\mathrm{ms}})}{\mathrm{ADC}_{44.5\mathrm{ms}}} \times 100(\%)$$

Where $ADC_{7.1ms}$ and $ADC_{44.5ms}$ represent the ADC values acquired using the OGSE and PGSE sequences, respectively.

ROI-based measurement

Commercially available software (Vitrea; Canon Medical Systems Corporation) was used for all image analyses. ADC maps were aligned with the postcontrast T1-weighted and FLAIR images using rigid body registration. Two independent radiologists (T.N. and J.K., with 10 and 8 years of radiological experience, respectively), who were blinded to the patients' clinical and pathological information, conducted an ROI analysis. A solid tumor component with significant enhancement was delineated using transverse contrast-enhanced T1-weighted images, whereas a nonenhancing solid tumor component was delineated utilizing transverse FLAIR images. The ROIs excluded tumor necrosis, cystic components, surrounding edema, macroscopic hemorrhage, and calcification. Subsequently, these ROIs were transferred to the corresponding ADC, cADC, and rcADC maps, which had been automatically registered to the postcontrast T1-weighted image employing Vitrea.

The mean $ADC_{44.5ms}$ ($ADC_{44.5\ ms}^{mean}$), $ADC_{7.1\ ms}$ ($ADC_{7.1\ ms}^{mean}$), cADC ($cADC^{mean}$), and rcADC ($rcADC^{mean}$) values were measured for the entire ROI. The minimum ADC value of gliomas correlated well with tumor cellularity, and that of HGGs was significantly lower than that of LGGs [30]. Therefore, we aimed to investigate the minimum and maximum ADC values of gliomas. In this study, ADC values were calculated pixel by pixel. To minimize the effects of noise, the 5th and 95th percentiles of each ADC distribution were identified, as this approach provided the lowest and highest robust values [30]. Therefore, the 5th and 95th percentile values of the $ADC_{44.5\ ms}$ ($ADC_{44.5\ ms}^{5th}$ and $ADC_{44.5ms}^{95th}$), $ADC_{7.1ms}$ ($ADC_{7.1ms}^{5th}$ and $ADC_{7.1ms}^{95th}$), cADC ($cADC^{5th}$ and $cADC^{95th}$), and rcADC ($rcADC^{5th}$ and $rcADC^{95th}$) were calculated.

Statistical analysis

The D'Agostino–Pearson normality test was used to assess the normality assumption for all parameters in all groups. Among the three groups, the one-way analysis of variance (ANOVA) was used to compare differences in age, Ki-67

LI, and time interval between MRI and surgery, whereas the chi-square test was utilized to compare differences in sex and CNS WHO grade. The intraclass correlation coefficient (ICC) was used to assess the interobserver agreement on parametric measurements, with an ICC of > 0.74 indicating excellent agreement [31]. Measurements from the two observers were averaged for each case and applied for subsequent analysis. Tumors were grouped based on the histopathological results. The mean values, as well as the 5th and 95th percentile values of the $ADC_{44.5ms}$, $ADC_{7.1ms}$, cADC, and rcADC, were compared as follows. For parameters with nonnormal distribution, the diffusion parameters between two groups were compared using the Kruskal–Wallis test; whereas, the diffusion parameters among three groups were compared using the Kruskal–Wallis test with the Bonferroni correction. Further, for parameters with normal distribution, the comparison between two groups was performed using ANOVA; whereas, comparison among three groups was conducted using ANOVA with the Bonferroni correction. A receiver operating characteristic (ROC) curve analysis was conducted to identify the optimum threshold for tumor differentiation and to measure the area under the ROC curve (AUC), sensitivity, specificity, and accuracy for determining *IDH*-wildtype gliomas or HGGs. Optimal $ADC_{44.5ms}$, $ADC_{7.1ms}$, cADC, and rcADC indices were selected. DeLong's test was used to compare the AUCs of the best-performing indices. The Bonferroni correction was applied for multiple comparisons. Further, we conducted multivariable logistic regression analyses to predict HGGs and *IDH*-wildtype gliomas. Candidate variables (age, sex, one conventional PGSE-based ADC index, and one rcADC index) were selected a priori based on clinical relevance and their diagnostic performance in the univariable analyses, and all selected variables were entered simultaneously (forced entry) in each multivariable model. As an internal validation, we assessed the stability of the model coefficients using 1,000 bootstrap resampling. In addition, the Hosmer–Lemeshow test was used to evaluate the calibration of the model. Spearman's rank correlation analysis was conducted to assess the association between the diffusion parameters and Ki-67 LI. The correlation was considered little or no relationship if $0 \le \rho < 0.25$, fair if $0.25 \le \rho < 0.5$, moderate to good if $0.5 \le \rho < 0.75$, and very good to excellent if $0.75 \le \rho$ [32]. Statistical analysis was conducted using a commercially available software package (MedCalc, version 15.10.0; MedCalc statistical software, IBM, version 28.0.1.0; IBM SPSS Statistics). Furthermore, statistical significance was set at p values of < 0.05.

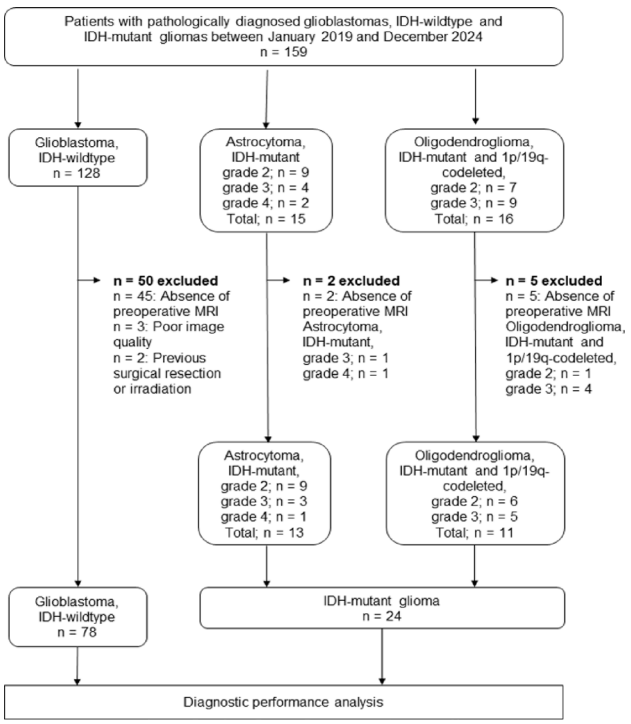

Fig. 1 Diagram indicating the inclusion and exclusion criteria and the flow of the inclusion of eligible patients in this study

Results

Patients

In this study, 159 consecutive patients, comprising (128 with glioblastoma, *IDH*-wildtype, CNS WHO grade 4; 9 with astrocytoma, *IDH*-mutant, CNS WHO grade 2; 4 with astrocytoma, *IDH*-mutant, CNS WHO grade 3; 2 with astrocytoma, *IDH*-mutant, CNS WHO grade 4; 7 with oligodendroglioma, *IDH*-mutant and *1p/19q*-codeleted, CNS WHO grade 2; and 9 with oligodendroglioma, *IDH*-mutant and *1p/19q*-codeleted, CNS WHO grade 3) were considered for inclusion. This study excluded 57 patients because of the absence of preoperative MRI, including both OGSE and PGSE DWI scans, poor image quality caused by artifacts in DWIs, or previous surgical resection or irradiation. This study analyzed 102 patients, comprising 78 with glioblastomas, *IDH*-wildtype, CNS WHO grade 4; and 24 with *IDH*-mutant gliomas (9 with astrocytoma, *IDH*-mutant, CNS WHO grade 2; 3 with astrocytoma, *IDH*-mutant, CNS WHO grade 3; 1 with astrocytoma, *IDH*-mutant, CNS WHO grade 4; 6 with oligodendroglioma, *IDH*-mutant and *1p/19q*-codeleted, CNS WHO grade 2; and 5 with oligodendroglioma, *IDH*-mutant and *1p/19q*-codeleted, CNS WHO grade 3) (Fig. 1). All glioblastomas, *IDH*-wildtype, CNS WHO grade 4, were enhancing lesions, except for one case. One case of astrocytoma, *IDH*-mutant, CNS WHO grade 4, was an enhancing lesion, whereas all astrocytomas, *IDH*-mutant, CNS WHO grades 3 and 2, were nonenhancing lesions. Three and two of oligodendrogliomas, *IDH*-mutant

and *1p/19q*-codeleted, CNS WHO grade 3, were enhancing and nonenhancing lesions, respectively. All oligodendrogliomas, *IDH*-mutant and *1p/19q*-codeleted, CNS WHO grade 2, were nonenhancing lesions. All patients were pathologically diagnosed after total or partial surgical resection. Table 1 presents the patients' demographic and pathological characteristics. A previous study compared glioblastomas and primary central nervous system lymphomas using time-dependent diffusion MRI [26]. Patients with glioblastoma analyzed in the present study involved 66 individuals who were included in our previous study. Sex did not differ among the three groups (p = 0.692). Age, CNS WHO grade, Ki-67 LI, and time interval between MRI and surgery significantly differed among the three groups (each $p <$ 0.001). Figures 2 and 3 illustrate the representative diffusion parametric maps of *IDH*-mutant glioma (LGG) and *IDH*-wildtype glioma (HGG).

Interobserver agreement

Supplementary Table 2 presents the ICCs and 95% confidence intervals (CIs) for each parameter. All parameters demonstrated excellent agreement.

Table 1 Patient demographic and pathological characteristics of patients

Characteristics	IDH-mutant 1p/19q-codeleted (n=11)	IDH-mutant 1p/19q-intact (n=13)	IDH-wildtype (n=78)	p value
Age (years)	50±10	42±14	70±13	<0.001
Sex (male/female)	7/4	9/4	45/33	0.692
CNS WHO grade				<0.001
Enhancement status				
Grade 2 enhanced/nonenhanced	6 (5.9%) 0/6 (0%/5.9%)	9 (8.8%) 0/9 (0%/8.8%)	0	
Grade 3 enhanced/nonenhanced	5 (4.9%) 3/2 (2.9%/2.0%)	3 (2.9%) 0/3 (0%/2.9%)	0	
Grade 4 enhanced/nonenhanced	0	1 (1.0%) 1/0 (1.0%/0%)	78 (76.5%) 77/1 (75.5%/1.0%)	
Ki-67 LI (%)	12.73±11.50	9.53±7.09	39.87±19.10	<0.001
Time interval between MRI and surgery (days)	9.45±6.89	34.77±56.24	6.03±5.86	<0.001

Values are expressed as numbers or mean±standard deviation

1p/19q chromosome arms 1p and 19q, *IDH* isocitrate dehydrogenase, *Ki-67* LI Ki-67 labeling index

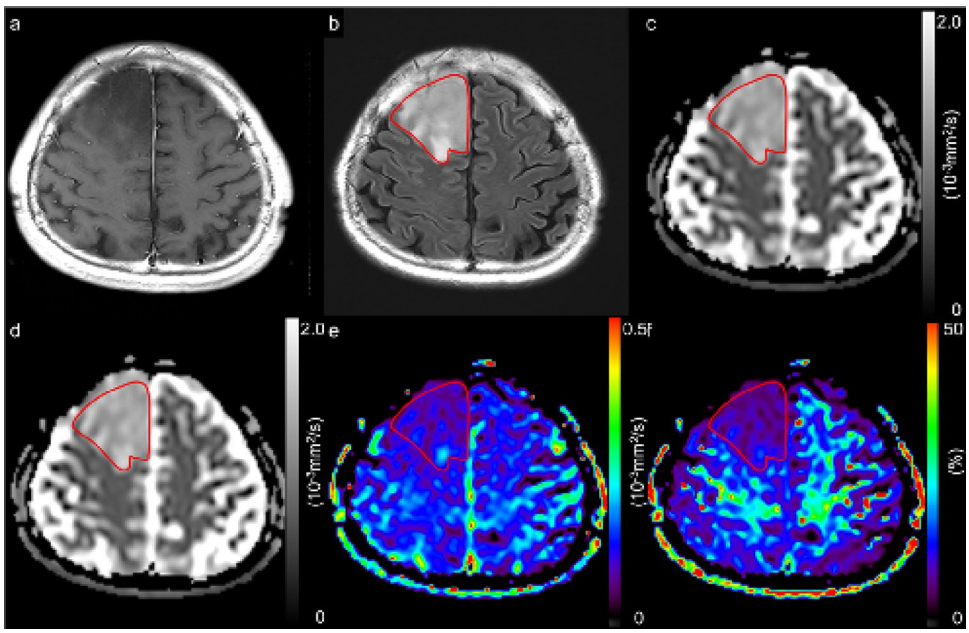

Fig. 2 A 53-year-old male patient with astrocytoma, *isocitrate dehydrogenase*-mutant, CNS WHO grade 2. A contrast-enhanced T1-weighted image demonstrated no contrast enhancement (**a**). A fluid-attenuated inversion recovery image with a ROI (solid line) (**b**). ADC maps derived from PGSE DWI at a Δ_{eff} of 44.5 ms (**c**) and from OGSE DWI at a Δ_{eff} of 7.1 ms (**d**). Maps of cADC (e) and rcADC (f) between PGSE and OGSE. Low cADC and rcADC levels in the tumor were observed. The mean $ADC_{44.5ms}$, $ADC_{7.1ms}$, cADC, and rcADC values are 1.271×10^{-3} mm^2/s, 1.323×10^{-3} mm^2/s, 0.052×10^{-3} mm^2/s, and 4.05%, respectively

Δ_{eff} effective diffusion time, *ADC* apparent diffusion coefficient, *cADC* apparent diffusion coefficient change, *DWI* diffusion-weighted imaging, *OGSE* oscillating-gradient spin-echo, *PGSE* pulsed-gradient spin-echo, *rcADC* relative apparent diffusion coefficient change

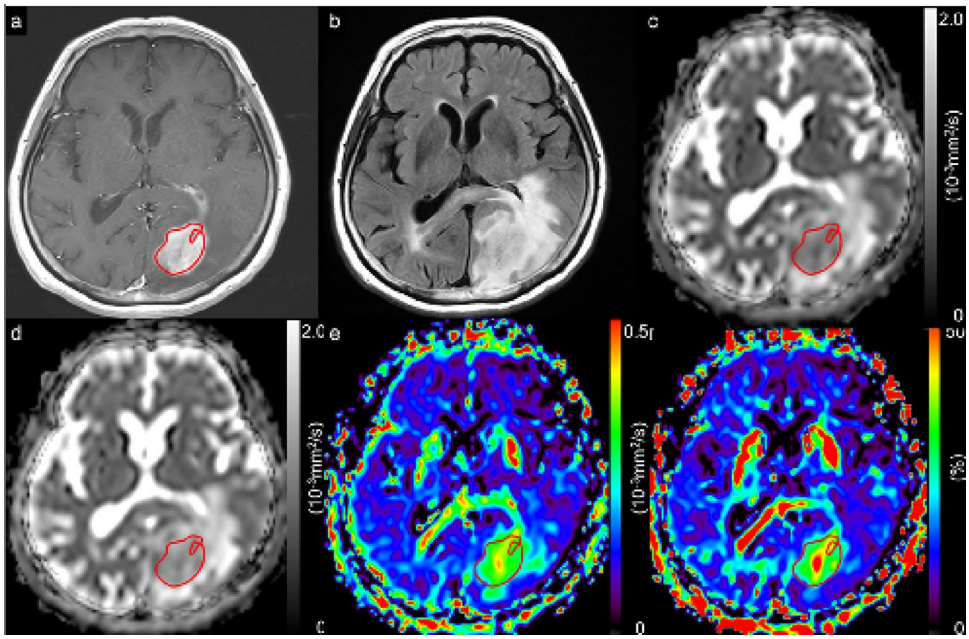

Fig. 3 A 70-year-old female patient with glioblastoma, *isocitrate dehydrogenase*-wildtype, CNS WHO grade 4. A contrast-enhanced T1-weighted image with a ROI (solid line) (**a**). A fluid-attenuated inversion recovery image (**b**). ADC maps derived from PGSE DWI at a Δ_{eff} of 44.5 ms (**c**) and from OGSE DWI at a Δ_{eff} of 7.1 ms (**d**). Maps of cADC (**e**) and rcADC (**f**) between PGSE and OGSE. High cADC and rcADC levels in the tumor were observed. The mean $ADC_{44.5ms}$, $ADC_{7.1ms}$, cADC, and rcADC values are 0.988×10^{-3} mm^2/s, 1.118×10^{-3} mm^2/s, 0.130×10^{-3} mm^2/s, and 13.9%, respectively
Δ_{eff} effective diffusion time, *ADC* apparent diffusion coefficient, *cADC* apparent diffusion coefficient change, *DWI* diffusion-weighted imaging, *OGSE* oscillating-gradient spin-echo, *PGSE* pulsed-gradient spin-echo, *rcADC* relative apparent diffusion coefficient change

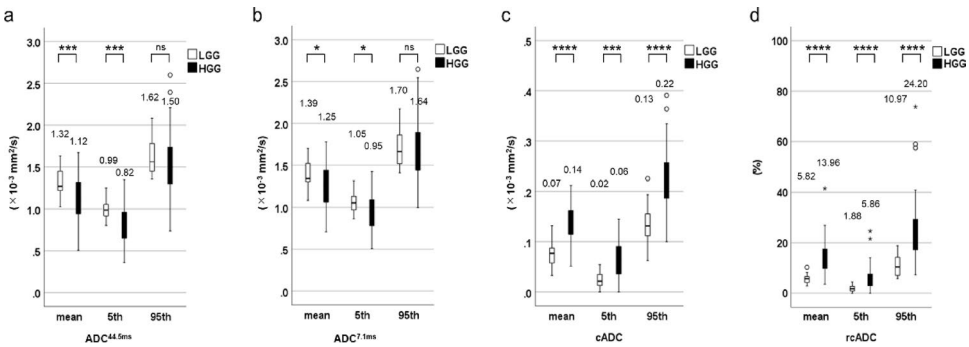

Fig. 4 Box and whisker plots of the mean, 5th percentile, and 95th percentile of the $ADC_{44.5ms}$ (**a**), $ADC_{7.1ms}$ (**b**), cADC (**c**), and rcADC (**d**) between pulsed-gradient spin-echo DWI and oscillating-gradient spin-echo DWI for LGGs and HGGs. The mean and 5th percentile of $ADC_{44.5ms}$ and $ADC_{7.1ms}$ were significantly lower for HGGs than for LGGs, and no significant difference was observed between LGGs and HGGs in the 95th percentile of $ADC_{44.5ms}$ and $ADC_{7.1ms}$ (**a**, **b**). All three indices of the cADC and rcADC values were significantly higher for HGGs than for LGGs (**c**, **d**). *$p<0.05$, **$p<0.01$, ***$p<0.005$, ****$p<0.001$
ADC apparent diffusion coefficient, *cADC* apparent diffusion coefficient change, *DWI* diffusion-weighted imaging, *HGG* high-grade gliomas, *LGG* low-grade gliomas, *rcADC* relative apparent diffusion coefficient change

Assessment of the diffusion parameters between LGGs and HGGs and among tumor grades

The mean and 5th percentile of the $ADC_{44.5ms}$ and $ADC_{7.1ms}$ were significantly lower for HGGs than for LGGs ($p=0.003$ for the $ADC_{44.5ms}^{mean}$, $p=0.001$ for the $ADC_{44.5ms}^{5th}$, $p=0.026$ for the $cADC^{mean}$, and $p=0.029$ for the $cADC^{5th}$), with no significant difference between the LGGs and HGGs in the 95th percentile of the $ADC_{44.5ms}$ and $ADC_{7.1ms}$ ($p=0.120$ and 0.422) (Fig. 4a and b). All three indices for the cADC and rcADC values were significantly higher for the HGGs than for the LGGs (each $p<0.001$) (Fig. 4c and d). Table 2 presents the results of the AUC, optimal threshold, sensitivity, specificity, and accuracy for the diffusion parameters of solid tumor components for differentiating LGGs and HGGs. The $ADC_{44.5ms}^{5th}$ (AUC: 0.762;

Table 2 The AUC, optimal threshold, sensitivity, specificity, and accuracy for the $ADC_{44.5ms}^{mean}$, $ADC_{44.5\ ms}^{5th}$, $ADC_{44.5\ ms}^{95th}$, $ADC_{7.1\ ms}^{mean}$, $ADC_{7.1ms}^{5th}$, $ADC_{7.1ms}^{95th}$, $cADC^{mean}$, $cADC^{5th}$, $cADC^{95th}$, $rcADC^{mean}$, $rcADC^{5th}$, and $rcADC^{95th}$ of the solid tumor component to differentiate between the low-grade and high-grade gliomas

Parameters	LGG ($n=15$)	HGG ($n=87$)	p-value	AUC (95% CI)	Threshold value	Sensitivity (%)	Specificity (%)	Accuracy (%)
$ADC_{44.5\ ms}^{mean}$	1.32±0.18 ($\times10^{-3}$ mm^2/s)	1.12±0.25 ($\times10^{-3}$ mm^2/s)	0.003	0.743 (0.646–0.824)	1.109 ($\times10^{-3}$ mm^2/s)	52.9	93.3	58.8
$ADC_{44.5\ ms}^{5th}$	0.99±0.12 ($\times10^{-3}$ mm^2/s)	0.82±0.21 ($\times10^{-3}$ mm^2/s)	0.001	0.762 (0.667–0.840)	0.862 ($\times10^{-3}$ mm^2/s)	56.3	93.3	61.8
$ADC_{44.5\ ms}^{95th}$	1.62±0.23 ($\times10^{-3}$ mm^2/s)	1.50±0.30 ($\times10^{-3}$ mm^2/s)	0.120	0.626 (0.525–0.720)	1.35 ($\times10^{-3}$ mm^2/s)	34.5	100	44.1
$ADC_{7.1\ ms}^{mean}$	1.39±0.18 ($\times10^{-3}$ mm^2/s)	1.25±0.24 ($\times10^{-3}$ mm^2/s)	0.026	0.680 (0.581–0.769)	1.289 ($\times10^{-3}$ mm^2/s)	57.5	80.0	60.8
$ADC_{7.1\ ms}^{5th}$	1.05±0.12 ($\times10^{-3}$ mm^2/s)	0.95±0.20 ($\times10^{-3}$ mm^2/s)	0.029	0.677 (0.578–0.767)	0.862 ($\times10^{-3}$ mm^2/s)	37.9	100	47.1
$ADC_{7.1\ ms}^{95th}$	1.70±0.24 ($\times10^{-3}$ mm^2/s)	1.64±0.29 ($\times10^{-3}$ mm^2/s)	0.422	0.565 (0.463–0.663)	1.433 ($\times10^{-3}$ mm^2/s)	253	93.3	35.3
$cADC^{mean}$	0.07±0.02 ($\times10^{-3}$ mm^2/s)	0.14±0.04 ($\times10^{-3}$ mm^2/s)	<0.001	0.919 (0.848–0.964)	0.093 ($\times10^{-3}$ mm^2/s)	88.5	93.3	89.2
$cADC^{5th}$	0.02±0.02 ($\times10^{-3}$ mm^2/s)	0.06±0.04 ($\times10^{-3}$ mm^2/s)	<0.001	0.810 (0.721–0.881)	0.055 ($\times10^{-3}$ mm^2/s)	60.9	100	66.7
$cADC^{95th}$	0.13±0.05 ($\times10^{-3}$ mm^2/s)	0.22±0.06 ($\times10^{-3}$ mm^2/s)	<0.001	0.882 (0.803–0.937)	0.157 ($\times10^{-3}$ mm^2/s)	87.4	80.0	86.3
$rcADC^{mean}$	5.82±2.01 (%)	13.96±5.94 (%)	<0.001	0.925 (0.855–0.967)	8.25 (%)	82.8	93.3	84.3
$rcADC^{5th}$	1.88±1.32 (%)	5.86±4.38 (%)	<0.001	0.816 (0.727–0.886)	4.45 (%)	60.9	100	66.7
$rcADC^{95th}$	10.97±4.46 (%)	24.20±10.95 (%)	<0.001	0.905 (0.831–0.954)	17.35 (%)	74.7	93.3	77.5

Values are expressed as mean±standard deviation

ADC apparent diffusion coefficient, *AUC* area under the receiver operating characteristic curve, *cADC* apparent diffusion coefficient change, *HGG* high-grade glioma, *LGG* low-grade glioma, *rcADC* relative apparent diffusion coefficient change

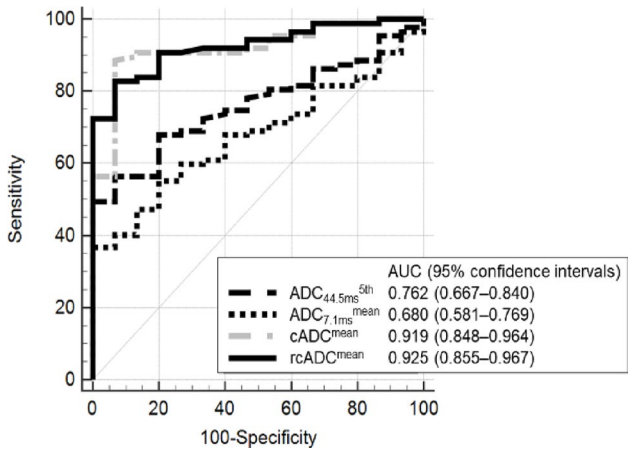

Fig. 5 Receiver operating characteristic curves for the best-performing $ADC_{44.5ms}$, $ADC_{7.1ms}$, cADC, and rcADC indices in the solid tumor component to differentiate between low-grade and high-grade gliomas *cADC* apparent diffusion coefficient change, *rcADC* relative apparent diffusion coefficient change

95% CI: 0.667–0.840), $ADC_{7.1ms}^{mean}$ (0.680; 0.581–0.769), $cADC^{mean}$ (0.919; 0.848–0.964), and $rcADC^{mean}$ (0.925; 0.855–0.967) values were the best-performing indices for $ADC_{44.5ms}$, $ADC_{7.1ms}$, cADC, and rcADC, respectively.

Table 3 Pairwise comparison of the AUCs among the $ADC_{44.5ms}^{5th}$, $ADC_{7.1ms}^{mean}$, $cADC^{mean}$, and $rcADC^{mean}$ in the solid tumor component to differentiate between low-grade and high-grade gliomas

Parameter	$rcADC^{mean}$	$cADC^{mean}$	$ADC_{7.1ms}^{mean}$
$ADC_{44.5\ ms}^{5th}$	0.163	0.157	0.081
DBA p	0.0015	0.0104	0.0955
$ADC_{7.1\ ms}^{mean}$	0.244	0.239	
DBA p	0.0001	0.0012	
$cADC^{mean}$	0.005		
DBA p	0.7658		

AUC area under the receiver operating characteristic curve, *cADC* apparent diffusion coefficient change, *DBA* difference between area under the receiver operating characteristic curve for each pair, *rcADC* relative apparent diffusion coefficient change

Figure 5 illustrates the ROC curves for $ADC_{44.5ms}^{5th}$, $ADC_{7.1ms}^{mean}$, $cADC^{mean}$, and $rcADC^{mean}$ values. The pairwise comparisons of AUCs among the best-performing indices revealed significantly higher AUCs of $rcADC^{mean}$ and $cADC^{mean}$ than those of $ADC_{44.5ms}^{5th}$ (AUC, 0.925, 0.919, and 0.762; $p=0.0015$, 0.0104) (Tables 2 and 3). Age, sex, $ADC_{44.5ms}^{5th}$, and $rcADC^{mean}$ were included in the model for the multivariable analysis predicting HGGs. In

the multivariable model for predicting HGGs, age and the rcADC^{mean} were retained as independent predictors. The adjusted odds ratio (OR) for age was 1.085 (95% CI: 1.027–1.146, $p=0.003$), and that for the rcADC^{mean} was 1.652 (95% CI: 1.194–2.285, $p=0.002$). The model achieved an AUC of 0.959 (95% CI: 0.923–0.996) with a classification accuracy of 91.2%. The stability of the coefficients was confirmed using bootstrap resampling (B = 1,000). Good calibration was confirmed using the Hosmer–Lemeshow test ($p=0.941$).

Supplementary Tables 3 and visualized in Supplementary Fig. 2 present the comparisons of diffusion parameters according to tumor grade. Significant differences in all ADC$_{44.5\ ms}$ indices among the three tumor grades were observed ($p=0.002$ for the ADC$_{44.5\ ms}^{mean}$, $p=0.003$ for the ADC$_{44.5ms}^{5th}$, and $p=0.037$ for the ADC$_{44.5\ ms}^{95th}$). The ADC$_{7.1ms}^{mean}$ demonstrated significant differences among the three tumor grades ($p=0.011$), except for the ADC$_{7.1\ ms}^{5th}$ and ADC$_{7.1\ ms}^{95th}$ ($p=0.052$ and 0.054). The ADC$_{44.5ms}^{mean}$, ADC$_{44.5\ ms}^{5th}$, and ADC$_{7.1\ ms}^{mean}$ values were significantly lower for CNS WHO grade 4 than for CNS WHO grade 2 ($p=0.004$, 0.005, and 0.048, respectively). All three indices of the cADC and rcADC were significantly higher for CNS WHO grade 4 than for CNS WHO grade 2 ($p=0.001$ for the cADC^{5th}, $p=0.004$ for the rcADC^{5th}, and $p<0.001$ for the others, respectively). No significant differences in any diffusion parameters were found between CNS WHO grades 3 and 4. Moreover, no significant difference in all the ADC$_{44.5ms}$ and ADC$_{7.1\ ms}$ indices was observed between CNS WHO grades 2 and 3. However, cADC^{mean}, cADC^{5th}, cADC^{95th}, rcADC^{mean}, and rcADC^{5th} were significantly higher CNS WHO grade 3 than for grade 2 ($p<0.001$, 0.002, 0.004, 0.018, and 0.015, respectively), except for the cADC^{95th} ($p=0.175$).

Assessment of diffusion parameters between *IDH*-mutant and *IDH*-wildtype gliomas and among tumor subtypes

All indices for ADC$_{44.5ms}$ and ADC$_{7.1ms}$ were significantly lower for *IDH*-wildtype gliomas than for *IDH*-mutant gliomas ($p<0.001$ for the ADC$_{44.5\ ms}^{mean}$, $p=0.001$ for the ADC$_{44.5ms}^{5th}$, $p=0.029$ for the ADC$_{44.5\ ms}^{95th}$, $p=0.003$ for the ADC$_{7.1ms}^{mean}$, and $p=0.012$ for the ADC$_{7.1ms}^{5th}$), except for ADC$_{7.1\ ms}^{95th}$ ($p=0.067$) (Figs. 6a and b). All three indices for the cADC and rcADC values were significantly higher for *IDH*-wildtype gliomas than for *IDH*-mutant gliomas ($p<0.001$ for cADC^{mean}, cADC^{95th}, rcADC^{mean}, and rcADC^{95th}; $p=0.032$ for the cADC^{5th}; and $p=0.015$ for the rcADC^{5th}) (Fig. 6c and d). Table 4 presents the AUC, optimal threshold, sensitivity, specificity, and accuracy for diffusion parameters of solid tumor components to differentiate between *IDH*-mutant and *IDH*-wildtype gliomas. The ADC$_{44.5ms}^{mean}$, ADC$_{7.1\ ms}^{mean}$, cADC^{mean}, and rcADC^{95th} values were the best-performing indices for ADC$_{44.5ms}$, ADC$_{7.1\ ms}$, cADC, and rcADC, respectively. Figure 7 illustrates the ROC curves for the ADC$_{44.5\ ms}^{mean}$ (AUC: 0.726, 95% CI: 0.629–0.810), ADC$_{7.1ms}^{mean}$ (0.701, 0.602–0.788), cADC^{mean} (0.746, 0.650–0.827), and rcADC^{95th} (0.807, 0.717–0.878) values. Pairwise comparisons of AUCs among the best-performing indices revealed that despite the highest performance of rcADC^{95th} (AUC: 0.807, 95% CI: 0.717–0.878), none of the AUC comparisons revealed significant differences (Table 5). At first, age, sex, ADC$_{44.5ms}^{mean}$, and rcADC^{95th} were included in the model for the multivariable analysis predicting *IDH*-wildtype gliomas. In the multivariable model for predicting *IDH*-wildtype gliomas, age and the rcADC^{95th} were retained as independent predictors. The adjusted OR for age was 1.125 (95% CI: 1.065–1.190, $p<0.001$), and that for the rcADC^{95th} was 1.149

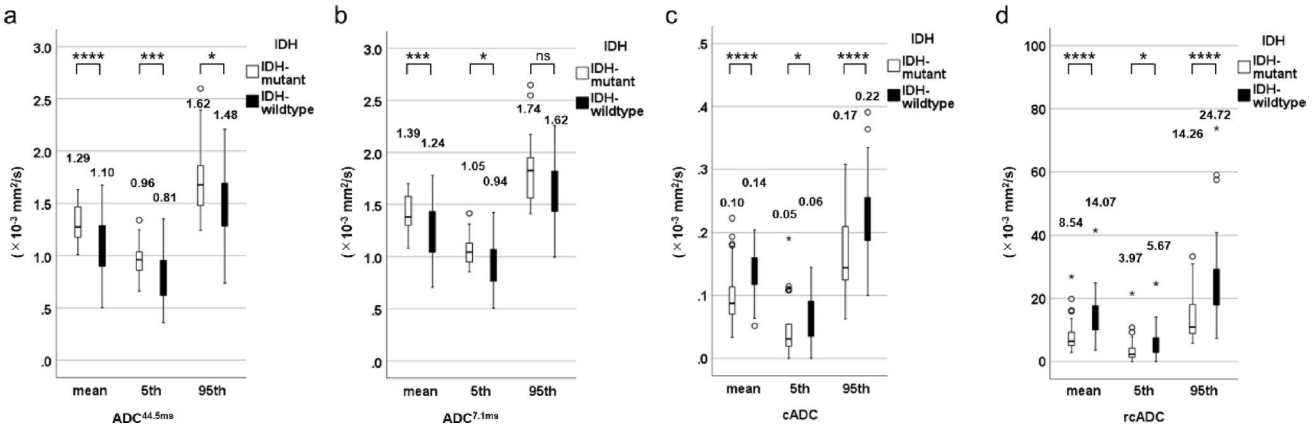

Fig. 6 Box and whisker plots of the mean, 5th percentile, and 95th percentile of ADC$_{44.5ms}$ (**a**), ADC$_{7.1ms}$ (**b**), cADC (**c**), and rcADC (**d**) between pulsed-gradient spin-echo and oscillating gradient spin-echo diffusion-weighted imaging for *isocitrate dehydrogenase* (*IDH*)-mutant and *IDH*-wildtype gliomas. *$p<0.05$, **$p<0.01$, ***$p<0.005$, ****$p<0.001$

cADC apparent diffusion coefficient change, *rcADC* relative apparent diffusion coefficient change

Table 4 The AUC, optimal threshold, sensitivity, specificity, and accuracy for the $ADC_{44.5\ ms}^{mean}$, $ADC_{44.5ms}^{5th}$, $ADC_{44.5\ ms}^{95th}$, $ADC_{7.1\ ms}^{mean}$, $ADC_{7.1\ ms}^{5th}$, $ADC_{7.1\ ms}^{95th}$, $cADC^{mean}$, $cADC^{5th}$, $cADC^{95th}$, $rcADC^{mean}$, $rcADC^{5th}$, and $rcADC^{95th}$ of the solid tumor component to differentiate between the IDH-mutant and IDH-wildtype gliomas

Parameters	IDH-mutant ($n=24$)	IDH-wildtype ($n=78$)	p	AUC (95% CI)	Threshold value	Sensitivity (%)	Specificity (%)	Accuracy (%)
$ADC_{44.5\ ms}^{mean}$	1.29 ± 0.20 ($\times 10^{-3}$ mm^2/s)	1.10 ± 0.24 ($\times 10^{-3}$ mm^2/s)	< 0.001	0.726 (0.629–0.810)	1.181 ($\times 10^{-3}$ mm^2/s)	65.4	75.0	67.6
$ADC_{44.5\ ms}^{5th}$	0.96 ± 0.16 ($\times 10^{-3}$ mm^2/s)	0.81 ± 0.21 ($\times 10^{-3}$ mm^2/s)	0.001	0.718 (0.621–0.803)	0.795 ($\times 10^{-3}$ mm^2/s)	50.0	91.7	59.8
$ADC_{44.5\ ms}^{95th}$	1.62 ± 0.26 ($\times 10^{-3}$ mm^2/s)	1.48 ± 0.30 ($\times 10^{-3}$ mm^2/s)	0.029	0.647 (0.547–0.739)	1.41 ($\times 10^{-3}$ mm^2/s)	47.4	83.3	55.9
$ADC_{7.1\ ms}^{mean}$	1.39 ± 0.18 ($\times 10^{-3}$ mm^2/s)	1.24 ± 0.23 ($\times 10^{-3}$ mm^2/s)	0.003	0.701 (0.602–0.788)	1.277 ($\times 10^{-3}$ mm^2/s)	59.0	79.2	63.7
$ADC_{7.1\ ms}^{5th}$	1.05 ± 0.15 ($\times 10^{-3}$ mm^2/s)	0.94 ± 0.20 ($\times 10^{-3}$ mm^2/s)	0.012	0.671 (0.571–0.761)	0.852 ($\times 10^{-3}$ mm^2/s)	38.5	100	52.9
$ADC_{7.1\ ms}^{95th}$	1.74 ± 0.24 ($\times 10^{-3}$ mm^2/s)	1.62 ± 0.29 ($\times 10^{-3}$ mm^2/s)	0.067	0.624 (0.523–0.718)	1.653 ($\times 10^{-3}$ mm^2/s)	60.3	66.7	61.8
$cADC^{mean}$	0.10 ± 0.05 ($\times 10^{-3}$ mm^2/s)	0.14 ± 0.04 ($\times 10^{-3}$ mm^2/s)	< 0.001	0.746 (0.650–0.827)	0.095 ($\times 10^{-3}$ mm^2/s)	89.7	75.0	86.3
$cADC^{5th}$	0.05 ± 0.05 ($\times 10^{-3}$ mm^2/s)	0.06 ± 0.04 ($\times 10^{-3}$ mm^2/s)	0.032	0.646 (0.545–0.738)	0.055 ($\times 10^{-3}$ mm^2/s)	61.5	79.2	65.7
$cADC^{95th}$	0.17 ± 0.07 ($\times 10^{-3}$ mm^2/s)	0.22 ± 0.06 ($\times 10^{-3}$ mm^2/s)	< 0.001	0.741 (0.644–0.822)	0.163 ($\times 10^{-3}$ mm^2/s)	85.9	62.5	80.4
$rcADC^{mean}$	8.54 ± 5.88 (%)	14.07 ± 5.79 (%)	< 0.001	0.796 (0.704–0.869)	8.25 (%)	85.9	75.0	83.3
$rcADC^{5th}$	3.97 ± 4.72 (%)	5.67 ± 4.12 (%)	0.015	0.665 (0.565–0.755)	4.45 (%)	61.5	79.2	65.7
$rcADC^{95th}$	14.26 ± 7.84 (%)	24.72 ± 11.05 (%)	< 0.001	0.807 (0.717–0.878)	14.75 (%)	87.2	66.7	82.4

Values are expressed as mean ± standard deviation

AUC area under the receiver operating characteristic curve, *cADC* apparent diffusion coefficient change, *IDH* isocitrate dehydrogenase, *rcADC* relative apparent diffusion coefficient change

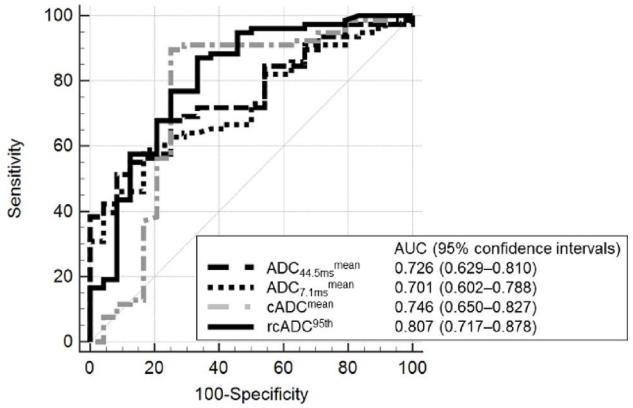

Fig. 7 Receiver operating characteristic curves for the best-performing $ADC_{44.5ms}$, $ADC_{7.1ms}$, cADC, and rcADC indices in the solid tumor component to differentiate between *isocitrate dehydrogenase*-mutant and *isocitrate dehydrogenase*-wildtype gliomas
cADC apparent diffusion coefficient change, *rcADC* relative apparent diffusion coefficient change

Table 5 Pairwise comparison of AUCs among the $ADC_{44.5ms}^{mean}$, $ADC_{7.1ms}^{mean}$, $cADC^{mean}$, and $rcADC^{95th}$ in the solid tumor component to differentiate between the IDH-mutant and IDH-wildtype gliomas

Parameter	$rcADC^{95th}$	$cADC^{mean}$	$ADC_{7.1ms}^{mean}$
$ADC_{44.5ms}^{mean}$	0.080	0.019	0.025
DBA	0.0879	0.7848	0.1183
p			
$ADC_{7.1ms}^{mean}$	0.106	0.045	
DBA	0.5901	0.5901	
p			
$cADC^{mean}$	0.061		
DBA	0.0715		
p			

ADC apparent diffusion coefficient, *AUC* area under the receiver operating characteristic curve, *cADC* apparent diffusion coefficient change, *DBA* difference between area under the receiver operating characteristic curve for each pair, *IDH* isocitrate dehydrogenase, *rcADC* relative apparent diffusion coefficient change

(95% CI: 1.026–1.286, $p=0.016$). The model achieved an AUC of 0.927 (95% CI: 0.872–0.983) with a classification accuracy of 92.2%. The stability of the coefficients was confirmed using bootstrap resampling (B = 1,000). Good calibration was confirmed by the Hosmer–Lemeshow test ($p=0.681$). Second, CNS WHO grade was added to the variables included in the multivariable analysis, in addition to age, sex, $ADC_{44.5ms}^{mean}$, and $rcADC^{95th}$. None of the variables, including age and $rcADC^{95th}$, were independent predictors. The adjusted OR for age was 7.787 (95% CI:

0–7.068E+101, $p=0.981$), and that for the $rcADC^{95th}$ was 52.214 (95% CI: 0–1.884E+216, $p=0.987$).

Supplementary Tables 4 and Fig. 3 illustrate the comparisons of diffusion parameters among the tumor subtypes. Significant differences in almost all diffusion parameters were observed among the three tumor subtypes ($p<0.001$ for $ADC_{44.5ms}^{mean}$, $ADC_{44.5ms}^{5th}$, $ADC_{7.1ms}^{mean}$, $cADC^{mean}$, $cADC^{95th}$, $rcADC^{mean}$, and $rcADC^{95th}$, $p=0.024$ for $ADC_{44.5ms}^{95th}$, $p=0.008$ for $ADC_{7.1ms}^{5th}$, $p=0.048$ for $ADC_{7.1ms}^{95th}$, and $p=0.032$ for $rcADC^{5th}$), except for $cADC^{5th}$ ($p=0.067$). $ADC_{44.5ms}^{mean}$, $ADC_{44.5ms}^{5th}$, $ADC_{44.5ms}^{95th}$, $ADC_{7.1ms}^{mean}$, and $ADC_{7.1ms}^{5th}$ were significantly lower for glioblastomas, *IDH*-wildtype, than for astrocytoma, *IDH*-mutant ($p<0.001$, < 0.001, 0.022, < 0.001, and 0.006, respectively), except for $ADC_{7.1ms}^{95th}$ ($p=0.056$). Moreover, $cADC^{mean}$, $cADC^{95th}$, $rcADC^{mean}$, and $rcADC^{95th}$ were significantly higher for glioblastomas, *IDH*-wildtype, than for astrocytoma, *IDH*-mutant (each $p<0.001$), except for $cADC^{5th}$ and $rcADC^{5th}$ ($p=0.129$ and 0.103). $ADC_{44.5ms}^{mean}$ and $ADC_{7.1ms}^{mean}$ values were significantly lower in the oligodendroglioma, *IDH*-mutant and *1p/19q*-codeleted than in the astrocytoma, *IDH*-mutant ($p=0.017$ and 0.028, respectively). No significant differences in other parameters were observed between the two tumor types. Furthermore, no significant differences in any diffusion parameters were found between glioblastomas, *IDH*-wildtype, and oligodendroglioma, *IDH*-mutant and *1p/19q*-codeleted.

Correlation between diffusion parameters and Ki-67 LI

The Ki-67 LI was significantly negatively correlated with $ADC_{44.5ms}^{mean}$, $ADC_{44.5ms}^{5th}$, $ADC_{7.1ms}^{mean}$, and $ADC_{7.1ms}^{5th}$, which was considered little to fair, except for $ADC_{44.5ms}^{95th}$ and $ADC_{7.1ms}^{95th}$. Moreover, it was significantly positively correlated with all cADC and rcADC indices, which were considered fair to good (Supplementary Table 5). The $rcADC^{mean}$ demonstrated the strongest correlation with the Ki-67 LI in these diffusion indices. Figure 8 illustrates the scatter plot of Ki-67 LI and $rcADC^{mean}$.

Discussion

This study revealed significantly higher time-dependent diffusion MRI parameters, including both the cADC and rcADC, in HGGs than in LGGs. The AUC of $rcADC^{mean}$ for differentiating between LGGs and HGGs was significantly higher than the AUCs of any conventional ADC-based index. Moreover, both cADC and rcADC were significantly higher for *IDH*-wildtype gliomas than for *IDH*-mutant gliomas. Of

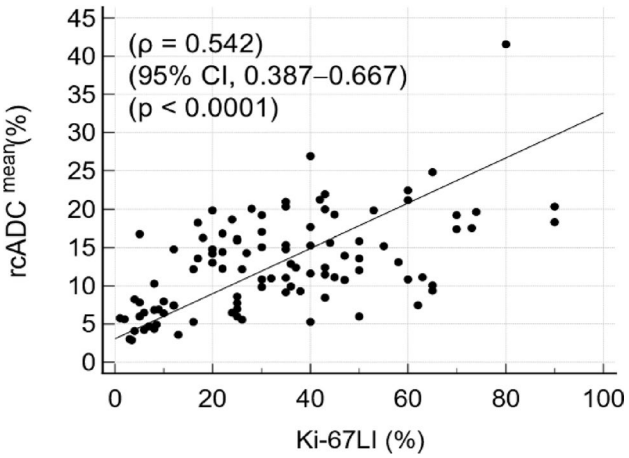

Fig. 8 Scatter plot illustrates the association between Ki-67 labeling index and rcADC. Significant positive correlation was noted between these parameters
rcADC relative apparent diffusion coefficient change

all indices, rcADC, particularly $rcADC^{95th}$, demonstrated the highest differentiating performance, although its superiority to conventional ADC-based indices was not statistically proven.

The clinical value of ADC in distinguishing HGGs from LGGs has been well documented. A distinctly low ADC in the solid tumor component of HGGs, which indicates higher cellularity and increased nuclear-to-cytoplasmic ratio, helps differentiate HGGs from LGGs [10−13]. Moreover, the ADC values distinguish *IDH*-wildtype gliomas from *IDH*-mutant gliomas. However, regarding the *1p/19q* codeletion status, the value of the ADC measurement remains unidentified [14−16].

Studies have investigated the application of time-dependent diffusion MRI in evaluating intracranial tumors. Maekawa et al. have demonstrated significantly higher cADC and rcADC between the short (6.5 ms) and long (32.5 ms) effective diffusion times in the high-grade intra-axial brain tumors than in the low-grade tumors [24]. More recently, Zhang et al. investigated pediatric gliomas using time-dependent diffusion MRI and used a two-compartment microstructural model to identify the intracellular fraction, cell diameter, and cellularity [33]. They revealed that the cellularity index provided the best performance in identifying the histological grade, whereas the cell diameter offered the most accurate differentiation for the molecular classification of *H3K27*-altered gliomas in midline gliomas. Moreover, Zhu et al. investigated five patients with glioma using an ultra-high-performance gradient MRI system and demonstrated that the ratio of the ADC measured at short diffusion times to that at long diffusion times holds promise for revealing heterogeneous tumor microstructures, including cellular density, in both presurgical and post-treatment gliomas [34]. These studies have revealed the clinical potential

and validity of time-dependent diffusion MRI for profiling intracranial tumors. However, no research has fully assessed the diagnostic performance of time-dependent diffusion MRI parameters in distinguishing HGGs from LGGs and *IDH*-wildtype gliomas from *IDH*-mutant gliomas compared with conventional ADC.

$ADC_{44.5ms}^{mean}$, $ADC_{44.5ms}^{5th}$, $ADC_{7.1ms}^{mean}$, and $ADC_{7.1ms}^{5th}$ values were significantly lower for HGGs than for LGGs, which is consistent with the results of previous studies [10−13], and all three indices of the cADC and rcADC values were significantly higher for HGGs than for LGGs. The pairwise comparisons of the AUCs for differentiating LGGs from HGGs revealed that the AUC of $rcADC^{mean}$ was significantly higher than that of $ADC_{44.5ms}^{5th}$, which was the best-performing ADC-based index. The differentiation of the three tumor grades revealed a significant difference in the conventional $ADC_{44.5ms}^{mean}$ between CNS WHO grades 2 and 4, despite no significant difference between CNS WHO grades 2 and 3 and between CNS WHO grades 3 and 4. Conversely, almost all cADC and rcADC parameters demonstrated significant differences between CNS WHO grades 2 and 3, except for $rcADC^{95th}$.

The Ki-67 LI serves as a marker of tumor cell proliferation, with increased values reflecting evaluated proliferative activity [35]. The present study revealed that the Ki-67 LI was negatively correlated with almost all ADC indices, except for $ADC_{44.5ms}^{95th}$ and $ADC_{7.1ms}^{95th}$, and positively correlated with all cADC and rcADC indices. Moreover, the $rcADC^{mean}$ demonstrated the strongest correlation, indicating that $rcADC^{mean}$ derived from time-dependent diffusion MRI may provide a more accurate assessment of glioma cell proliferation, which may explain the better differentiation performance between LGGs and HGGs.

The differentiation between *IDH*-mutant and *IDH*-wildtype gliomas indicated that all three indices of $ADC_{44.5ms}$ and $ADC_{7.1ms}$ were significantly lower for *IDH*-wildtype gliomas than for *IDH*-mutant gliomas. The $ADC_{44.5ms}^{mean}$ and $ADC_{7.1ms}^{mean}$ values of oligodendrogliomas (*IDH*-mutant and *1p/19q*-codeleted gliomas) were significantly lower than those of astrocytomas (*IDH*-mutant gliomas with intact *1p/19q*). These results are consistent with those of previous studies [14−16]. All *IDH*-wildtype gliomas are classified as CNS WHO grade 4, which is characterized by a higher cellularity [2]. This may explain why *IDH*-wildtype gliomas have lower ADC values than *IDH*-mutant gliomas. However, why intermediate ADC values were observed in the *1p/19q*-codeleted gliomas remains unknown. Regarding the time-dependent diffusion MRI parameters, all three indices of the cADC and rcADC values were significantly higher for *IDH*-wildtype gliomas than for *IDH*-mutant gliomas. A similar trend was observed across all three indices of cADC and rcADC values in differentiating LGGs from HGGs. However, the diagnostic performance of rcADC was reduced. The *IDH*-mutant gliomas include HGGs such as astrocytoma, *IDH*-mutant, CNS WHO grade 3 and 4, and oligodendroglioma, *IDH*-mutant and *1p/19q*-codeleted, CNS WHO grade 3. The pathological features of high-grade *IDH*-mutant and *IDH*-wildtype gliomas show considerable overlap [2]. These tumors are associated with higher cellularity and an increased nuclear-to-cytoplasmic ratio compared with CNS WHO grade 2 tumors [2], which may have led to higher rcADC values. Age, sex, $ADC_{44.5ms}^{mean}$, and $rcADC^{95th}$ were included in the model for the multivariable analysis predicting *IDH*-wildtype gliomas, in which $rcADC^{95th}$ and age were identified as independent predictors. Furthermore, CNS WHO grade was added to the variables included in the multivariable analysis, none of the variables, including age and $rcADC^{95th}$, were independent predictors. This may be due to a strong correlation between CNS WHO grade and imaging markers or age, as well as the influence of multicollinearity resulting from the limited number of cases. From a clinical application perspective, CNS WHO grade is not identified preoperatively; therefore, a predictive model based on imaging markers without including CNS WHO grade would be more practical. In this study, $rcADC^{95th}$, as an independent predictor of *IDH*-wildtype gliomas after adjusting for age and sex was useful for distinguishing *IDH*-wildtype from *IDH*-mutant gliomas.

Limitations of the study

This study has several limitations. First, the sample size was relatively small. Thus, studies with larger sample sizes are warranted to confirm our findings. Second, we measured ROIs under two different conditions, including enhancing and nonenhancing compartments. This may be affecting the ADC measurement. A more standardized method for setting ROIs is expected. Third, only two effective diffusion times (7.1 ms and 44.5 ms) and a fixed set of b-values (0 and 1,500 s/mm^2) were examined. The use of shorter or longer effective diffusion times may have affected the results. However, the gradient performance of our clinical MRI system limited the range of effective diffusion time in OGSE. An MRI system with higher gradients may help achieve a shorter effective diffusion time in OGSE. Finally, all tumors were pathologically diagnosed; however, the detailed comparisons between the tissue microstructures and imaging findings were not performed.

Conclusions

The study demonstrates that rcADC indices derived from time-dependent diffusion MRI outperform conventional PGSE-based ADC parameters in glioma characterization. Specifically, $rcADC^{mean}$ shows a strong correlation with Ki-67 LI and serves as an independent predictor of HGGs, while $rcADC^{95th}$ independently differentiates *IDH*-wildtype from *IDH*-mutant gliomas. These findings highlight the value of rcADC indices for improved noninvasive assessment of glioma grade and molecular status.

Supplementary Information The online version contains supplementary material available at https://doi.org/10.1007/s11604-025-01936-w.

Acknowledgements The authors would like to thank the staff of Kagoshima University Hospital for their support and Enago (www.enago.jp) for the English language review.

Funding This work was supported by JSPS KAKENHI Grant Number JP23K07113.

References

1. Report of Brain Tumor Registry of Japan. Brain tumor registry of Japan (2005–2008). Neurol Med Chir. 2017;57:9–102. https://doi.org/10.2176/nmc.sup.2017-0001.
2. Brat DJ, Ellison DW, Figarella-Branger D, Hawkins CE, Louis DN, Perry A, et al. Gliomas, glioneuronal tumors, and neuronal tumors. WHO classification of tumors editorial board. WHO classification of tumors of the central nervous system. 5th ed. Lyon: International agency for research on cancer; 2021. pp. 15–187.
3. Hartmann C, Hentschel B, Wick W, Capper D, Felsberg J, Simon M, et al. Patients with IDH1 wild type anaplastic astrocytomas exhibit worse prognosis than those with IDH1-mutated glioblastomas, and the IDH1 mutation status accounts for the unfavorable prognostic effect of higher age: implications for the classification of gliomas. Acta Neuropathol. 2010;120:707–18. https://doi.org/10.1007/s00401-010-0781-z.
4. Bell EH, Zhang P, Shaw EG, Buckner JC, Barger GR, Bullard DE, et al. Comprehensive genomic analysis in NRG oncology/RTOG 9802: a phase III trial of radiation versus radiation plus procarbazine, lomustine (CCNU), and vincristine in high-risk low-grade glioma. J Clin Oncol. 2020;38:3407–17. https://doi.org/10.1200/JCO.19.02983.
5. Li J, Niu X, Gan Y, Yang Y, Wang T, Zhang H, et al. Clinical and pathological features and prognostic factors for recurrent gliomas. World Neurosurg. 2019;128:e21–30. https://doi.org/10.1016/j.wneu.2019.02.210.
6. Freije WA, Castro-Vargas FE, Fang Z, Horvath S, Cloughesy T, Liau LM, et al. Gene expression profiling of gliomas strongly predicts survival. Cancer Res. 2004;64:6503–10. https://doi.org/10.1158/0008-5472.CAN-04-0452.
7. Johannessen AL, Torp SH. Clinical value of the Ki-67/MIB-1 labeling index in human astrocytomas. Pathol Oncol Res. 2006;12:143–7. https://doi.org/10.1007/BF02893360.
8. Gutt-Will M, Murek M, Schwarz C, Hewer E, Vulcu S, Beck J, et al. Frequent diagnostic under-grading in isocitrate dehydrogenase wild-type gliomas due to small pathological tissue samples. Neurosurgery. 2019;85:689–94. https://doi.org/10.1093/neuros/nyy433.
9. Chen L, Liu M, Bao J, Xia Y, Zhang J, Zhang L, et al. The correlation between apparent diffusion coefficient and tumor cellularity in patients: a meta-analysis. PLoS ONE. 2013;8:e79008. https://doi.org/10.1371/journal.pone.0079008.
10. Yan R, Haopeng P, Xiaoyuan F, Jinsong W, Jiawen Z, Chengjun Y, et al. Non-Gaussian diffusion MR imaging of glioma: comparisons of multiple diffusion parameters and correlation with histologic grade and MIB-1 (Ki-67 labeling) index. Neuroradiology. 2016;58:121–32. https://doi.org/10.1007/s00234-015-1606-5.
11. Wang QP, Lei DQ, Yuan Y, Xiong NX. Accuracy of ADC derived from DWI for differentiating high-grade from low-grade gliomas: systematic review and meta-analysis. Medicine. 2020;99:e19254. https://doi.org/10.1097/MD.0000000000019254.
12. Phuttharak W, Thammaroj J, Wara-Asawapati S, Panpeng K. Grading glioma capability: comparison between visual assessment and apparent diffusion coefficient (ADC) value measurement on diffusion-weighted imaging (DWI). Asian Pac J Cancer Prev. 2020;21:385–90. https://doi.org/10.31557/APJCP.2020.21.2.385.
13. Momeni F, Abedi-Firouzjah R, Farshidfar Z, Taleinezhad N, Ansari L, Razmkon A, et al. Differentiating between low- and high-grade glioma tumors by measuring the apparent diffusion coefficient values in various regions of the brain. Oman Med J. 2021;36:e251. https://doi.org/10.5001/omj.2021.59.
14. Nuessle NC, Behling F, Tabatabai G, Castaneda Vega S, Schittenhelm J, Ernemann U, et al. ADC-based stratification of molecular glioma subtypes using high b-value diffusion-weighted imaging. J Clin Med. 2021;10:3451. https://doi.org/10.3390/jcm10163451.
15. Ma X, Cheng K, Cheng G, Li C, Lyu J, Lan Y, et al. Apparent diffusion coefficient as an imaging biomarker of IDH mutation, 1p19q codeletion, and MGMT promoter methylation status in patients with glioma. J Magn Reson Imaging. 2023;58:732–8. https://doi.org/10.1002/jmri.28589.
16. Wang X, Shu X, He P, Cai Y, Geng Y, Hu X, et al. Ultra-high b-value DWI accurately identifies isocitrate dehydrogenase genotypes and tumor subtypes of adult-type diffuse gliomas. Eur Radiol. 2024;34:6751–62. https://doi.org/10.1007/s00330-024-10708-5.
17. Baron CA, Beaulieu C. Oscillating gradient spin-echo (OGSE) diffusion tensor imaging of the human brain. Magn Reson Med. 2014;72:726–36. https://doi.org/10.1002/mrm.24987.
18. Portnoy S, Fichtner ND, Dziegielewski C, Stanisz MP, Stanisz GJ. In vitro detection of apoptosis using oscillating and pulsed gradient diffusion magnetic resonance imaging. NMR Biomed. 2014;27:371–80. https://doi.org/10.1002/nbm.3070.
19. Wu D, Martin LJ, Northington FJ, Zhang J. Oscillating gradient diffusion MRI reveals unique microstructural information in normal and hypoxia-ischemia injured mouse brains. Magn Reson Med. 2014;72:1366–74. https://doi.org/10.1002/mrm.25441.

20. Pyatigorskaya N, Le Bihan D, Reynaud O, Ciobanu L. Relationship between diffusion time and diffusion MRI signal observed at 17.2 Tesla in the healthy rat brain cortex. Magn Reson Med. 2014;72:492–500. https://doi.org/10.1002/mrm.24921.
21. Stejskal EO, Tanner JE. Spin diffusion measurements: spin echoes in the presence of a time-dependent field gradient. J Chem Phys. 1965;42:288–92. https://doi.org/10.1063/1.1695690.
22. Stejskal EO. Use of spin echoes in a pulsed magnetic-field gradient to study anisotropic, restricted diffusion and flow. J Chem Phys. 1965;43:3597–603. https://doi.org/10.1063/1.1696526.
23. Iima M, Yamamoto A, Kataoka M, Yamada Y, Omori K, Feiweier T, et al. Time-dependent diffusion MRI to distinguish malignant from benign head and neck tumors. J Magn Reson Imaging. 2019;50:88–95. https://doi.org/10.1002/jmri.26578.
24. Maekawa T, Hori M, Murata K, Feiweier T, Kamiya K, Andica C, et al. Differentiation of high-grade and low-grade intraaxial brain tumors using time-dependent diffusion MRI. Magn Reson Imaging. 2020;72:34–41. https://doi.org/10.1016/j.mri.2020.06.018.
25. Kamimura K, Kamimura Y, Nakano T, Hasegawa T, Nakajo M, Yamada C, et al. Differentiating brain metastasis from glioblastoma using time-dependent diffusion MRI. Cancer Imaging. 2023;23:75. https://doi.org/10.1186/s40644-023-00595-2.
26. Kamimura K, Nakano T, Hasegawa T, Nakajo M, Yamada C, Kamimura Y, et al. Differentiating primary central nervous system lymphoma from glioblastoma by time-dependent diffusion using oscillating gradient. Cancer Imaging. 2023;23:114. https://doi.org/10.1186/s40644-023-00639-7.
27. Kamimura K, Tokuda T, Kamizono J, Nakano T, Hasegawa T, Nakajo M, et al. Time-dependent MR diffusion analysis of functioning and nonfunctioning pituitary adenomas/pituitary neuroendocrine tumors. J Neuroimaging. 2025;35:e13254. https://doi.org/10.1111/jon.13254.
28. Higa N, Akahane T, Yokoyama S, Yonezawa H, Uchida H, Takajo T, et al. A tailored next-generation sequencing panel identified distinct subtypes of wildtype IDH and TERT promoter glioblastomas. Cancer Sci. 2020;111:3902–11. https://doi.org/10.1111/cas.14597.
29. Does MD, Parsons EC, Gore JC. Oscillating gradient measurements of water diffusion in normal and globally ischemic rat brain. Magn Reson Med. 2003;49:206–15. https://doi.org/10.1002/mrm.10385.
30. Chung WJ, Kim HS, Kim N, Choi CG, Kim SJ. Recurrent glioblastoma: optimum area under the curve method derived from dynamic contrast-enhanced T1-weighted perfusion MRI. Radiology. 2013;269:561–8. https://doi.org/10.1148/radiol.13130016.
31. Shrout PE, Fleiss JL. Intraclass correlations: use for assessing rater reliability. Psychol Bull. 1979;86:420–8. https://doi.org/10.1037/0033-2909.86.2.420.
32. Woo S, Lee JM, Yoon JH, Joo I, Han JK, Choi BI. Intravoxel incoherent motion diffusion-weighted MRI of hepatocellular carcinoma: correlation with degree of enhancement and histologic grade. Radiology. 2014;270:758–67. https://doi.org/10.1148/radiol.13130444.
33. Zhang H, Liu K, Ba R, Zhang Z, Zhang Y, Chen Y, et al. Histological and molecular classifications of pediatric gliomas using time-dependent diffusion MRI based microstructural mapping. Neuro Oncol. 2023;25:1146–56. https://doi.org/10.1093/neuonc/noad003.
34. Zhu A, Shih R, Huang RY, DeMarco JK, Bhushan C, Morris HD, et al. Revealing tumor microstructure with oscillating diffusion-encoding MRI in presurgical and posttreatment glioma patients. Magn Reson Med. 2023;90:1789–801. https://doi.org/10.1002/mrm.29758.
35. Fisher BJ, Naumova E, Leighton CC, Naumov GN, Kerklviet N, Fortin D, et al. Ki-67: a prognostic factor for low-grade glioma? Int J Radiat Oncol Biol Phys. 2002;52:996–1001. https://doi.org/10.1016/s0360-3016(01)02720-1.

Authors and Affiliations

Kiyohisa Kamimura[1] · Tsubasa Nakano[2] · Masanori Nakajo[2] · Junki Kamizono[2] · Tomohito Hasegawa[2] · Daiki Tobo[2] · Akie Mukai[2] · Yoshiki Kamimura[2] · Fumitaka Ejima[2] · Hiroaki Nagano[2] · Koji Takumi[2] · Masatoyo Nakajo[2] · Nayuta Higa[3] · Hajime Yonezawa[3] · Ryosuke Hanaya[3] · Mari Kirishima[4] · Akihide Tanimoto[4] · Hirokazu Otsuka[5] · Daisuke Hirahara[6] · Hiroshi Imai[7] · Thorsten Feiweier[8] · Takashi Yoshiura[1]

✉ Kiyohisa Kamimura
kiyohisa@m2.kufm.kagoshima-u.ac.jp

[1] Department of Advanced Radiological Imaging, Kagoshima University Graduate School of Medical and Dental Sciences, 8-35-1, Sakuragaoka, Kagoshima 890-8544, Japan

[2] Department of Radiology, Kagoshima University Graduate School of Medical and DentalSciences, 8-35-1, Sakuragaoka, Kagoshima 890-8544, Japan

[3] Departmentof Neurosurgery, Kagoshima University Graduate School of Medicaland Dental Sciences, 8-35-1, Sakuragaoka, Kagoshima 890-8544, Japan

[4] Department of Pathology, KagoshimaUniversity Graduate School of Medical and Dental Sciences, 8-35-1, Sakuragaoka, Kagoshima 890-8544, Japan

[5] Department of Radiological Technology, Kagoshima University Hospital, 8-35-1, Sakuragaoka, Kagoshima 890-8544, Japan

[6] Department of AI Research Lab, Harada Academy, 2-54-4, Higashi-Tanayama, Kagoshima 891-0113, Japan

[7] Siemens Healthcare K.K., Gate City Osaki West Tower, 1-11-1, Shinagawa-ku, Tokyo, Osaki 141-8644, Japan

[8] Research & Clinical Translation, Magnetic Resonance, Siemens Healthineers AG, Allee am Roethelheimpark 2, Erlangen 91052, Germany